applied sciences

MDPI

Article

Optical Design Study with Uniform Field of View Regardless of Sensor Size for Terahertz System Applications

Jungjin Park [1], Jaemyung Ryu [1,*] and Hojong Choi [2,*]

[1] Department of Optical Engineering, Kumoh National Institute of Technology, 350-27 Gumi-daero, Gumi 39253, Republic of Korea; wjdwls3875@naver.com
[2] Department of Electronic Engineering, Gachon University, 1342 Seongnam-daero, Sujeong-gu, Seongnam 13120, Republic of Korea
* Correspondence: jmryu@kumoh.ac.kr (J.R.); hojongch@gachon.ac.kr (H.C.); Tel.: +82-54-478-7778 (J.R.); +82-31-750-5591 (H.C.)

Abstract: The focal length in a typical optical system changes with the angle of view, according to the size of the sensor. This study proposed an optical terahertz (THz) system application where the focal length changed while the angle of view was fixed; thus, the image height was variable and responded to various sensor sizes. Therefore, it is possible to respond to various sensors with one optical system when the inspection distance is fixed. The fundamental optical system was designed by arranging the refractive power, which was determined according to the sensor size using the Gaussian bracketing method. A zoom optical system that changed the image height by fixing the angle of view and changed the focal length by moving the internal lens group was designed. THz waves exhibit minimal change in the refractive index depending on the wavelength. Moreover, their long-wavelength characteristics facilitate the development of millimeter-level pixel sizes. Therefore, the root mean square size of the maximum spot was 0.329 mm, which corrected the aberration to less than 1 mm (smaller than the pixel size). Further, a lighting analysis at 3 and 6 m locations confirmed the expansion of the lighting area by the magnification of the sensor size. After turning off certain light sources, we checked the contrast ratio via lighting analysis and confirmed that the size of one pixel was clearly distinguishable. Consequently, this newly designed optical system performed appropriately as an optical inspection system for THz system applications.

Keywords: zoom optical system; fixed angle of view; terahertz applications

Citation: Park, J.; Ryu, J.; Choi, H. Optical Design Study with Uniform Field of View Regardless of Sensor Size for Terahertz System Applications. *Appl. Sci.* **2024**, *14*, 9097. https://doi.org/10.3390/app14199097

Academic Editor: Zhi-Ting Ye

Received: 17 September 2024
Revised: 4 October 2024
Accepted: 6 October 2024
Published: 8 October 2024

1. Introduction

A Terahertz (THz) wave is a type of electromagnetic wave ranging 0.1–10 THz (wavelength range of 30–3000 μm) [1,2]. There is an unexplored frequency range between optically accessible light waves and electronically accessible radio or millimeter waves in the electromagnetic range [3]. THz waves exhibit unique physical characteristics, including superior penetrability compared to radio frequency waves (electromagnetic waves of the shortest wavelength) and the straight-line nature of light waves (far-infrared rays of the longest wavelength) [4,5]. As electromagnetic waves, THz waves are harmless to the human body and transmit light through non-metallic materials such as fibers and plastic. Therefore, they can be used for imaging tests as they reflect greatly on the skin and exhibit absorbency for soft biological media that cannot be filtered using X-rays [6]. In addition, THz waves are sensitive to the macroscopic behavior of molecules and chemical bonds. Therefore, their low-quantum mechanical energy is being studied for various applications in biochemistry and life sciences [7]. THz applications include high-speed/high-capacity short-range communication networks for the next-generation Internet of Things, security, medical imaging, agriculture, semiconductors, biochemistry, life sciences, and display manufacturing for crack detection [8,9]. The materials that refract THz waves are limited and are used to focus waves within a specific area [10,11]. In THz applications, mechanical

parts made of such materials exhibit a lens shape similar to that of general visual light [12]. The shape and thickness of a single lens and the arrangement of multiple lenses must be determined to focus the THz wave at the desired location with the desired energy distribution [13]. These processes are assumed to be the same as those used in the design process of a general optical system.

In typical optical systems, an object is never fixed at a certain position; thus, a focus control function is essential [14–16]. This optical system for THz applications is characterized by almost no wavelength-dependent change in the refractive index, and the wavelength is very long; therefore, the pixel size of the imaging device is also very large. Consequently, the size of the imaging device becomes very large with the increase in the number of pixels compared to that of a general visible-light imaging device. Therefore, only imaging devices with fewer pixels than the quarter video graphics array (QVGA) class should be developed. For a pixel size of 1 mm, even if it was in the QVGA class, the size of the imaging device is a considerably larger area than that of a general visible-light imaging device. Currently, there is no standardized sensor size for THz applications, and several companies are developing various sensor sizes. Therefore, optical system design tailored to a certain fixed sensor size may be difficult to apply to another sensor size. In an inspection optical system, the inspection distance is usually fixed. If the sensor size changes, the field of view must be fixed. However, our proposed optical system with a fixed field of view can respond to various sensor sizes. In addition, no problems are encountered if the optical aberration is corrected only at the millimeter level. Thus, the optical system must be designed using optical system design software (CODE V 2023.03), and its performance must be evaluated using design software [17,18]. Accordingly, the proposed optical system must be designed to respond to imaging devices of varying sizes. However, in these optical systems, the inspection distance and range are generally fixed. Therefore, an optical system with a fixed angle of view and variable imaging element size must be developed.

In the last 15 years, studies related to lens fabrication using metamaterials or optical system designs for THz applications have been scarce. An aspherical lens was fabricated using polyethylene to obtain a large numerical aperture for THz imaging applications [19]. Using photolithography, an ultrathin lens was fabricated to obtain a large axial focal depth for THz applications [20]. Further, an ultrathin meta-surface multi-focus lens device comprising C-shaped antenna units was designed to have 2 or 3 mm focal spacing, thereby covering a range of 0.3–1.1 THz [21]. Using a three-dimensional printer, a lens group was fabricated based on a ridge prism to produce monochromatic light and a diffraction-free length within the THz range [22]. Using polymer materials, an f-θ lens covering a wide field of view was fabricated to obtain heterogeneous samples and provide a constant phase over a 34° field of view (FOV) for 0.3–1.0 THz [23]. Using silicon material, an achromatic meta-lens composed of silicon pillars was fabricated for 0.6–1.0 THz [24]. Using a two-dimensional material, a tunable optical magnetic lens was fabricated to focus on the photon beam range and tune the phase shift [25]. A diffractive lens with concentric rings was fabricated using a three-dimensional printer to generate specific diffraction patterns for THz applications [26].

This study designed a novel optical zoom system with a fixed angle of view to support various imaging device sizes for THz applications. To accommodate imaging devices of various sizes, a zoom optical system was constructed wherein the image height was variable, the angle of view was fixed, and the focal length was changed. Based on the optimized design, the lens shape was improved, and aberrations were corrected. The focal length was varied using an internal focus movement method in which the overall length was fixed, and the internal lens group was moved to reduce problems such as driving weight or noise. Because the position of the sensor must be fixed, the focus is adjusted by calculating the amount of movement of the lens group using the zoom equation. Because of the nature of THz waves, their transmittance is very high; therefore, there is a strong possibility that sensor pixels will develop to be larger than 1 mm. Thus, the performance of the optical system was confirmed using a spot diagram. Infinite object points at both

3 and 6 m were confirmed according to the object distance in the spot diagram. In addition, the size of the focus was confirmed within 1 mm for all zooms at the wide-angle, middle, and telephoto ends. The largest focus was 0.329 mm at the telephoto end when the object distance was 3 m. Distortion was also checked at infinite object points of 3 and 6 m, depending on the object's distance. The distortion value and grid chart were checked for all zooms at the wide angle, middle, and telephoto ends. Because aberrations can be confirmed at the millimeter level, the performance was analyzed using light tools and a lighting optical system software package. The receivers were installed at object distances of 3 and 6 m, and lighting analysis was performed with a light source array at the sensor location. Because the size of the sensor was very large, a light source array of approximately 1/10 the size of the sensor was placed in the center and peripheral portions of the entire sensor size, and the illumination was checked at the central and peripheral receivers. The target lighting area enlarged by the magnification of the sensor was satisfactory for all zooms. The lighting analysis conducted after turning off certain lights indicated that the size of each pixel was clearly distinguished, and the contrast ratio was high in all zooms. Thus, the performance of the inspection optical system was satisfactory. The new optical system proposed in this study can be used regardless of the sensor size, thereby broadening the inspection range.

Based on our research and previous studies, this is the first study to design a zoom optical system with a fixed angle of view that can support various imaging device sizes for THz applications. The primary contributions of this new design are as follows.

1. The optical system proposed for THz applications can have various focal lengths while maintaining the same angle of view by setting a fixed angle of view. A single optical system can support various sensor sizes, thereby reducing optical system design and manufacturing costs. The first lens group was designed with a positive power such that consistent brightness could be maintained at the wide-angle and telephoto ends.

2. The focus was adjusted while maintaining the overall optical field by moving a specific internal lens group. This reduced the weight of the driving lens group, broadened the range of motor choices, and improved inspection speed.

The remainder of this paper is organized as follows. Section 2 describes the design and analysis of a zoomed-in optical system used in THz applications. Section 3 describes the performance analysis of the designed zoom optical system, including spot diagrams, distortion, and illumination analysis. Finally, Section 4 concludes the paper and summarizes the designed optical system.

2. Methods

In general, a zoom optical system refers to an optical system wherein the magnification changes continuously, the position of the image surface is fixed, and the focal length changes based on the object distance variance [27,28]. As shown in Figure 1a, in an optical system wherein the size of the imaging element is fixed, the focal length is short and long at the wide-angle and telephoto ends, respectively, and varies depending on the angle of view. If the angle of view is fixed in a zoom optical system designed following the conventional method, the maximum height of the chief ray in the image plane changes, as shown in Figure 1b. The focal distance and image height exhibit a proportional relationship [29–31]. When the angle of view is fixed, the image height decreases at short focal distances and increases at long focal distances [32,33]. Using this phenomenon, if the angle of view is fixed as per the size of the imaging element proposed in the THz optical system, the focal length of the optical system changes according to the size of the imaging element.

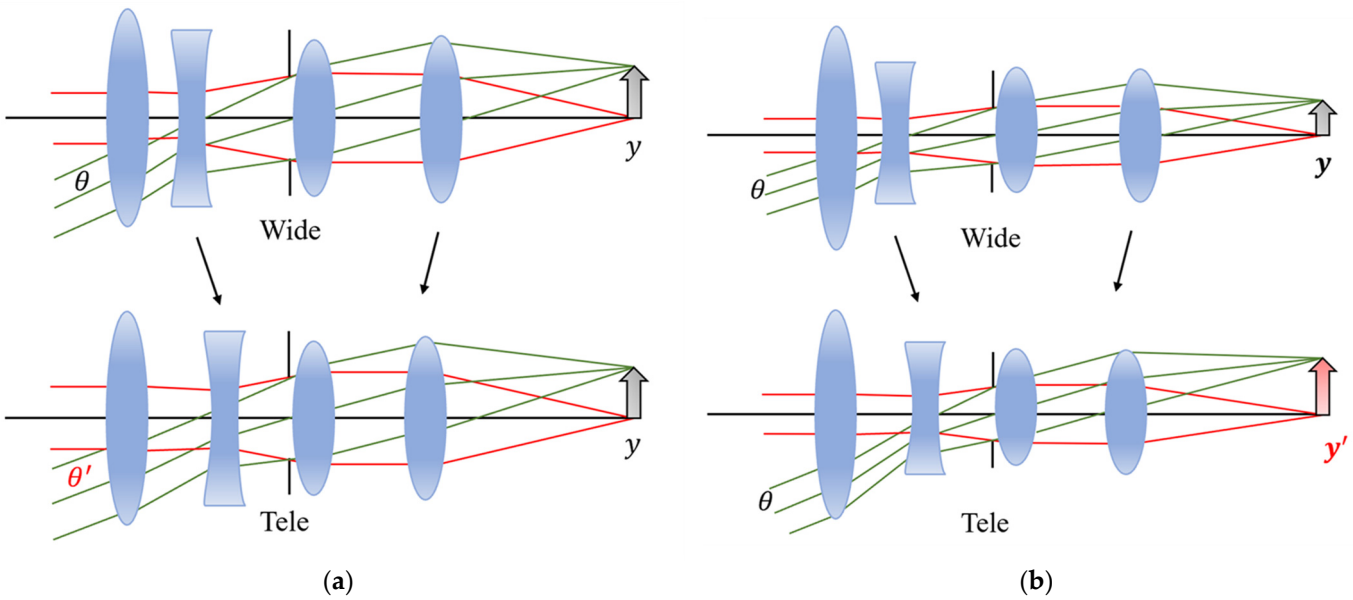

(**a**) (**b**)

Figure 1. Relationship between focal length and angle of view in (**a**) general optical system and (**b**) optical system for THz applications.

Figure 2 illustrates the relationship between the focal length and angle of view, where, θ, y, and $H2$ are the half angle of view, image height, and location of the second major surface, respectively, and f is the effective focal length (EFL), which is the distance from the second principal plane to the focal point.

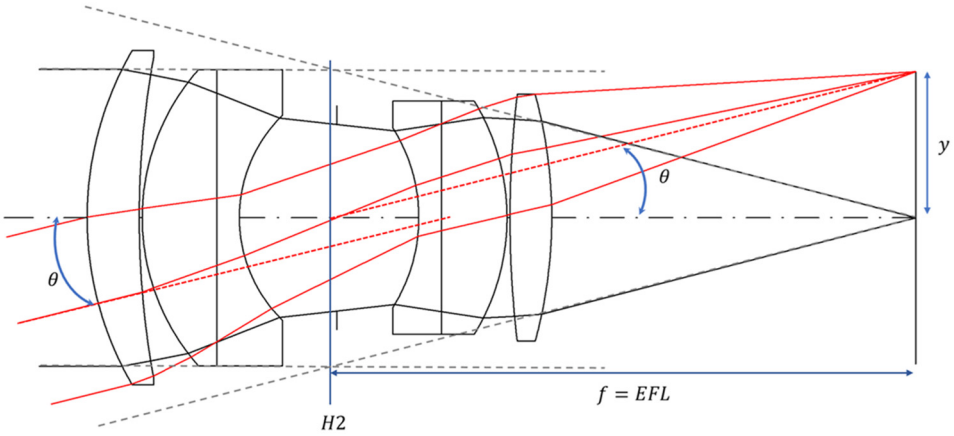

Figure 2. Relationship between focal length and field of view.

The maximum angle of incidence of the chief ray is referred to as the half FOV (HOF), which indicates the range that can be achieved in the optical system. The half angle of the view was determined by the maximum size of the imaging device [34]. The half-angle size y of the imaging device is expressed as Equation (1).

$$y = f \cdot \tan\theta, \tag{1}$$

where θ and f are the half angle of view and the focal length, respectively.

In general, the size of an imaging device is fixed; therefore, the angle of view of the optical system is determined by the focal length of the optical system. As shown in Equation (1), the angle of view decreases, the focal length increases, and vice versa. Figure 3 shows the angle of view according to the focal length of the optical system.

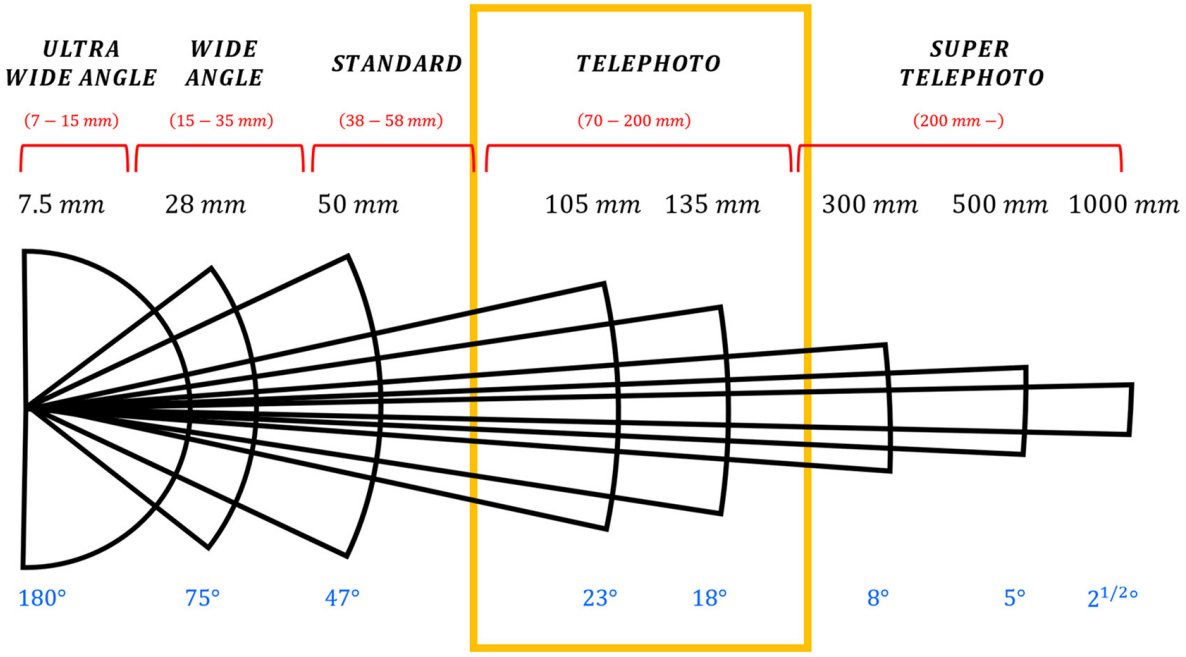

Figure 3. The angle of view is according to the focal length.

In general optics, a lens with a focal length of 50 mm is referred to as a standard lens [35]. Compared with a standard lens, an optical system with a larger angle of view and a shorter focal length of 35 mm or less is referred to as a wide-angle lens, and an optical system with a smaller angle of view and a longer focal length of 70 mm or more is called a telephoto lens. However, the proposed optical system had a fixed angle of view and large image height; thus, the focal length is greater than 50 mm. Therefore, the mode with a relatively small focal length, owing to the relatively small size of the image, is referred to as the wide-angle end, and the mode with a relatively long focal length is referred to as the telephoto end. Our proposed optical system has a field of view in the telephoto range.

Equivalent lenses refer to lenses with different axial thicknesses but the same total refractive power and paraxial optical properties regarding peripheral rays. The process of converting a specific lens into an equivalent lens of a different thickness is referred to as equivalent lens conversion, which is useful for the initial design or local changes in optical systems [36]. A lack of change in the paraxial optical properties indicates that the total refractive power and height at which the paraxial ray enters the principal plane are the same. The equivalent lens transformation conditions can be expressed as a quadratic equation. Therefore, no solution may exist. Having two real roots implies that another solution exists with the same thickness and characteristics, albeit with a different radius of curvature.

Figure 4 shows the optical path diagram of a thick lens where n is the refractive index, h is the height of the ray incident on the principal plane, H is the principal point, u is the paraxial angle, and its subscript refers to the plane number. Further, l and l' are the object and image distances, respectively, and z refers to the position of the principal surface.

According to the analytical equivalent lens transformation method, the height of incidence on the principal plane does not change. Using this concept, the heights of the h_1 and h_2 incidents on each side of Figure 4 can be expressed using Equation (2).

$$\begin{aligned} h_1 &= h - zu_0 = h - \left(\frac{n_0 u_0 d_1}{n_1 K}\right) k_2 \\ h_2 &= h - z' u_2 = h + \left(\frac{n_2 u_2 d_1}{n_1 K}\right) k_1 \end{aligned} \tag{2}$$

where k and K are the refractive powers of the relevant surface and the entire lens, respectively. By substituting Equation (2) into the refraction equation in Equation (3), we obtain Equation (4).

$$n_{i+1}u_{i+1} = n_i u_i - h_{i+1}k_{i+1} \tag{3}$$

$$\begin{aligned} \left(h - \frac{d_1 n_0 u_0 k_2}{n_1 K}\right)k_1 &= n_0 u_0 - n_1 u_1 \\ \left(h + \frac{d_1 n_{1+1} u_{1+1} k_1}{n_1 K}\right)k_2 &= n_1 u_1 - n_2 u_2 \end{aligned} \tag{4}$$

Equation (4) is a nonlinear simultaneous equation for k_1 and k_2. When the k_1 and k_2 terms are eliminated, they are expressed as a simultaneous linear equation in Equation (5).

$$k_2 = \frac{n_1 u_1 K - n_2 u_2 k_1}{n_0 u_0} \tag{5}$$

The simultaneous equations in Equation (5) are converted into quadratic equations for k_1, as shown in Equation (6), and the solution to this equation becomes an equivalent lens.

$$\frac{n_2 u_2 d_1}{n_1 K}k_1^2 + (h - d_1 u_1)k_1 + n_1 u_1 - n_0 u_0 = 0 \tag{6}$$

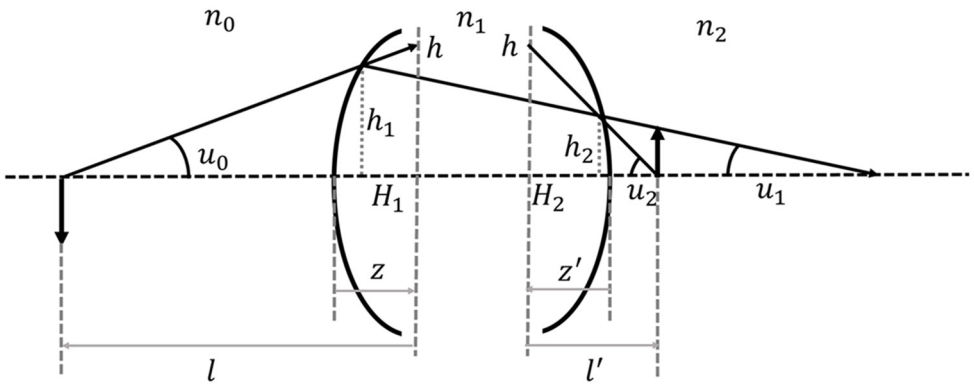

Figure 4. Thick single-lens optical layout at finite point.

The inspection distance and range of the optical system must be fixed. For a zoom optical system, the position of the image surface must be fixed; therefore, the internal lens or specific lens group has to be moved [37,38]. An internal focus control method was used to fix the position of the image surface and move the internal focus control group to the target inspection distance such that the overall length of the optical system did not change. Further, Group 1 in the optical system must be arranged to have a positive refractive power. This is because there should be no difference in brightness between the wide-angle and telephoto ends.

In this study, the CODE V (Synopsis Inc., East Boothbay, ME, USA) optical design software was used to determine the angle of view corresponding to the three types of imaging devices proposed in the THz wavelength range, and the optical system was constructed by arranging the refractive power of each lens. We aimed to design an optical system wherein the angle of view was fixed, and only a specific lens group was moved such that the image height varied depending on the size of the imaging element. Aberration is not a problem if it is smaller than the array size of the detection module. Therefore, the optical aberration must be corrected at the millimeter level. Further, we aimed to conduct a performance analysis by checking the contrast ratio of the pixels using Light Tools (Synopsis Inc.), which is a lighting optical design software package.

As the wavelength in the THz band is very long, the pixel size is considerably larger than that of a visible-light pixel. An imaging device becomes very large if the number of pixels increases; therefore, only imaging devices with a low number of pixels are expected to be developed. A wide-angle end with a short focal length and a telephoto end with a

long focal length is required to construct a zoom lens with a variable focal length. This is also referred to as the normal or middle stage between the wide-angle and the telephoto ends. As presented in Table 1, we aimed to construct an optical system that supported three types of imaging devices: wide-angle, telephoto, and intermediate ends.

Table 1. The image detector proposed in this study.

Detector	Number of Pixels	Pixel Size (mm)
Wide	64 × 64	1.5
Middle	128 × 128	1
Tele	200 × 100	1

The reciprocal of the focal length of a lens is known as the refractive power or the power of the lens. If the refractive power is positive, a positive refractive power is obtained and vice versa. When indicating the type, the previous abbreviations were used and written as P (positive) and N (negative). In this optical system, the first group was determined to have a positive refractive power, such that the brightness of the wide-angle and telephoto ends was maintained. A Group 4 lens with the refractive power of the PNPP (a lens arrangement of positive–negative–positive–positive) was designed as the basis. Our optical system utilized the Gaussian bracket method to express the total refractive power and that overall length using Equation (7). Here, z is the distance between the principal surfaces of each lens group, k is the refractive power of each lens group, K is the refractive power of the entire lens, and T is the total length of the optical system. Further, the subscripts k and z represent the lens group numbers. The focal length of the optical system was determined by the sensor size of the wide-angle and telephoto ends of the imaging device, as expressed in Equation (7). Because the reciprocal of the focal length is the refractive power of the optical system, K_1 and K_2 are the refractive powers at the wide-angle and telephoto ends, respectively.

$$\begin{gathered} [k_1, -z_{1,1}, k_2, -z_{1,2}, k_3, -z_{1,3}, k_4] = K_1 \\ [k_1, -z_{1,1}, k_2, -z_{1,2}, k_3, -z_{1,3}, k_4, -z_{1,4}] = 0 \\ [k_1, -z_{2,1}, k_2, -z_{2,2}, k_3, -z_{2,3}, k_4] = K_2 \\ [k_1, -z_{2,1}, k_2, -z_{2,2}, k_3, -z_{2,3}, k_4, -z_{2,4}] = 0 \\ z_{1,1} + z_{1,2} + z_{1,3} + z_{1,4} = T \\ z_{2,1} + z_{2,2} + z_{2,3} + z_{2,4} = T \end{gathered} \tag{7}$$

By solving the above Gaussian bracketing method and arranging the refractive power, the optical system was composed of four groups. Figure 5 shows an optical path diagram of a zoom lens wherein the image height was fixed in the form of a general zoom lens, and the angle of view changed such that the lens group moved and the focal length changed. It had a fixed whole length that utilized an internal focus movement method to move between Groups 2 and 4.

For the fundamental optical system design with a refractive power arrangement, a spot diagram was checked to confirm the optical system performance. Figure 6a–c show the spot diagrams at the wide-angle, middle, and telephoto ends, respectively, in the case of an infinite object distance. The x-axis of the spot diagram represents the defocusing range, and the y-axis represents the maximum image height standardized to 1, indicating the number of fields. Because the pixel size of the sensor exceeded 1 mm, a 1 mm × 1 mm square border was placed and checked to determine whether it was larger than the pixel size.

As shown in Figure 6, the boundary line was exceeded in all zoomed cases. Further, lens shape improvement and aberration correction were required; therefore, performance improvement is required to obtain a focus smaller than the pixel size.

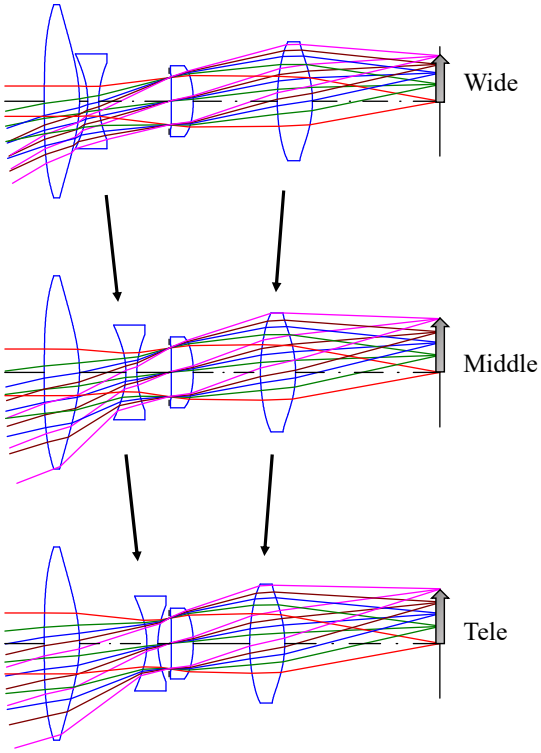

Figure 5. The fundamental layout of the zoom optical system is based on the placement of refractive power.

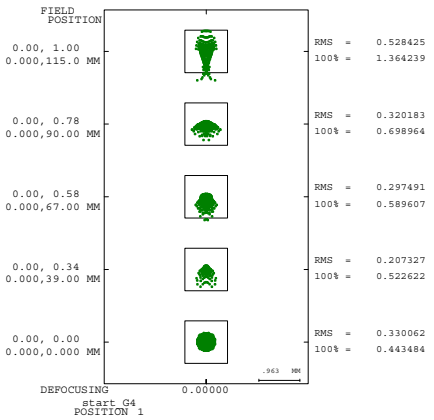

(**a**)

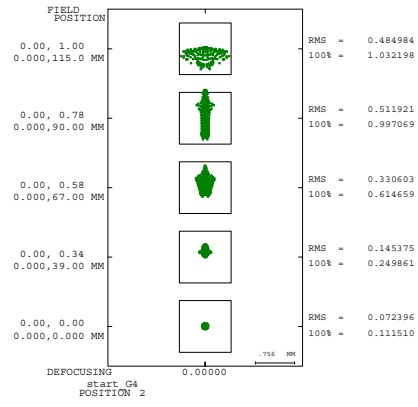

(**b**)

Figure 6. *Cont.*

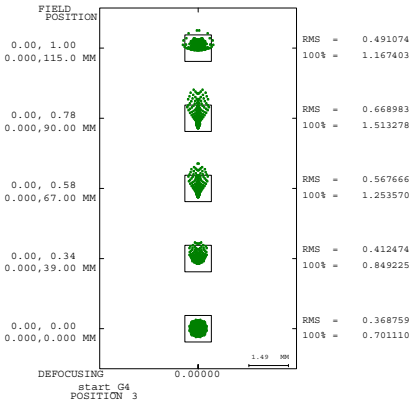

(**c**)

Figure 6. Spot diagrams at (**a**) wide, (**b**) middle, and (**c**) tele ends.

3. Results

A variable-field zoom lens was constructed using a fundamental optical system designed by arranging the refractive power. Four aspheric lenses were constructed using TPX material, with the first lens having a diameter of approximately 16 inches. TPX is advantageous for aberration correction due to its minimal variation in refractive index across different wavelengths. Subsequently, the design was optimized to improve the lens shape and aberration correction. In a zoom optical system, the sensor generally does not change; therefore, the image height is fixed. However, the proposed optical system was responsive to various imaging devices. Therefore, the image height calculated from the size of the imaging device, as presented in Table 1, was set for each zoom.

Figure 7 shows the optical path diagram for each zoom of the optical system designed with four lenses for infinite object distance. In Figure 7, the optical system is composed of a four-element, four-group lens with a PNPP configuration, so the focal length for each lens group is indicated at the infinity-wide end. The focal length of the first, second, third, and fourth lenses is 974.72 mm, –201.88 mm, 425.71 mm, and 320.44 mm, respectively. As evident, the size of the image height changed for each zoom as Groups 2 and 4's lenses moved. As evident, the size of the image height changed for each zoom as Groups 2 and 4's lenses moved. As the focal length changed, the distance between groups changed continuously.

An internal focus-shifting method was used to change the focal length using an internal lens. This is because the overall length of the optical system did not change. The optical system comprised four lenses. Groups 1, 2, 3, and 4 were the focator, variator, relay, and compensator, respectively. It was an optical system wherein Groups 1 and 3 were fixed, Group 2 functioned as the regulator and changed the focal length, and Group 4 t functioned as the compensator compensated for the amount of lens movement in Group 2. As the height of view was variable, the angle of view was fixed. The zoom magnification, calculated as the ratio of the focal length at the wide-angle end to that at the telephoto end, was approximately 1.23 times. Because of the large size of the image, it was difficult to obtain the same angle of view for all zooms. Therefore, the optical system was designed by determining the angle of view that minimized the difference between the angles of view at the wide-angle and telephoto ends. The difference in the FOV between the wide-angle and telephoto ends was approximately 6°. Excluding the FOV difference due to distortion, the FOV difference was approximately 0.2 times the FOV at the telephoto end, which is not sufficiently significant to cause detection issues.

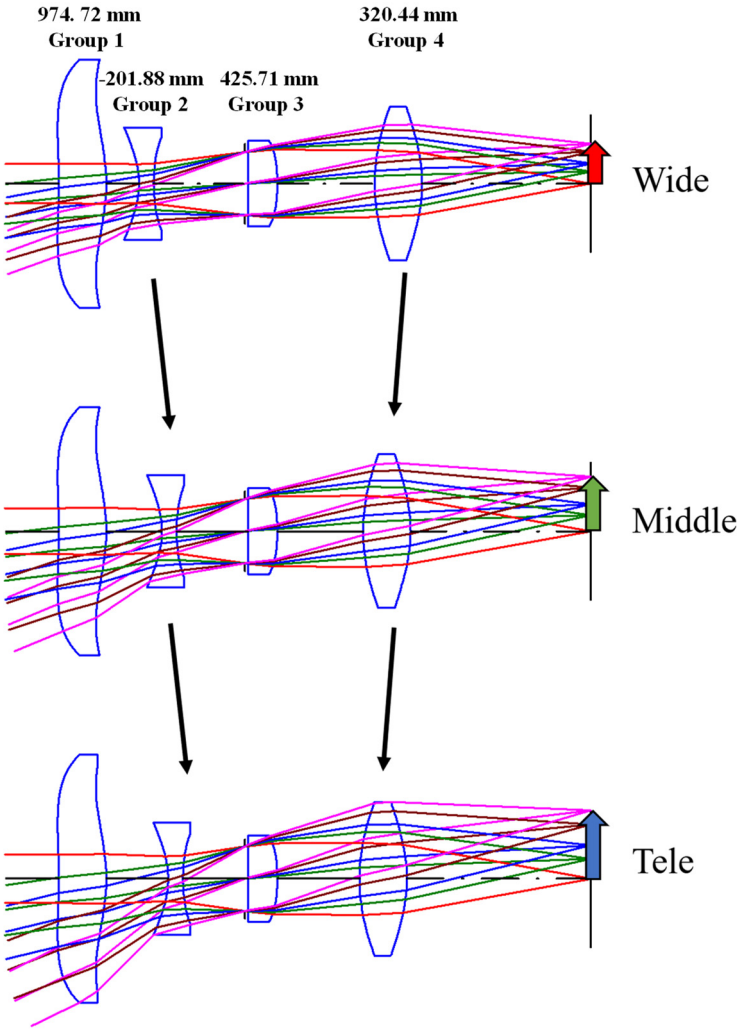

Figure 7. Optical path diagram for height-variable zoom lens.

A continuous line drawing the movement path of each group is referred to as the zoom locus. Figure 8 shows the zoom locus of a variable-height zoom lens programmed with Macro Plus, a built-in macro in CODE V software (Ver. 2023.03). The *x*-axis represents the total length of the optical system at a distance in millimeters. The *y*-axis represents the movement amount of the linear movement group, and is the cam angle normalized to one at the telephoto end. Each line shows the locus of movement volume for each group. Groups 1 and 3 remained fixed. Thus, there was no movement, and the lines were drawn straight. Group 2 was a variator, and its focal length changed from the wide-angle to the telephoto end. Therefore, changed linearly. Group 4 moved linearly to compensate for the movement of Group 2. In addition, the image line on the top surface was fixed as a straight line because the overall length was fixed when using the internal focus movement method.

The performance of the optical system must be evaluated through lighting analysis. If the distortion aberration of the optical system is large, the peripheral area may become blurred during the lighting analysis. Therefore, the target distortion value was determined to be within 5% using the optimized design.

As shown in Figures 9–11, the distortion aberration at each zoom according to the object distance using a distortion grid was verified. In a distortion grid chart, the *x*- and *y*-axes represent the long- and short-change angles, respectively. The red grid line, which represents the actual FOV, is the actual image created using the optical system, and the black grid line (Paraxial FOV) is the standard image. The larger the difference between the two grid lines, the greater the distortion. The shape wherein the center of the image

appears to protrude outward is referred to as the barrel type, and that wherein the center of the image appears to be pressed inward and the edges appear to bulge outward is referred to as the pincushion type.

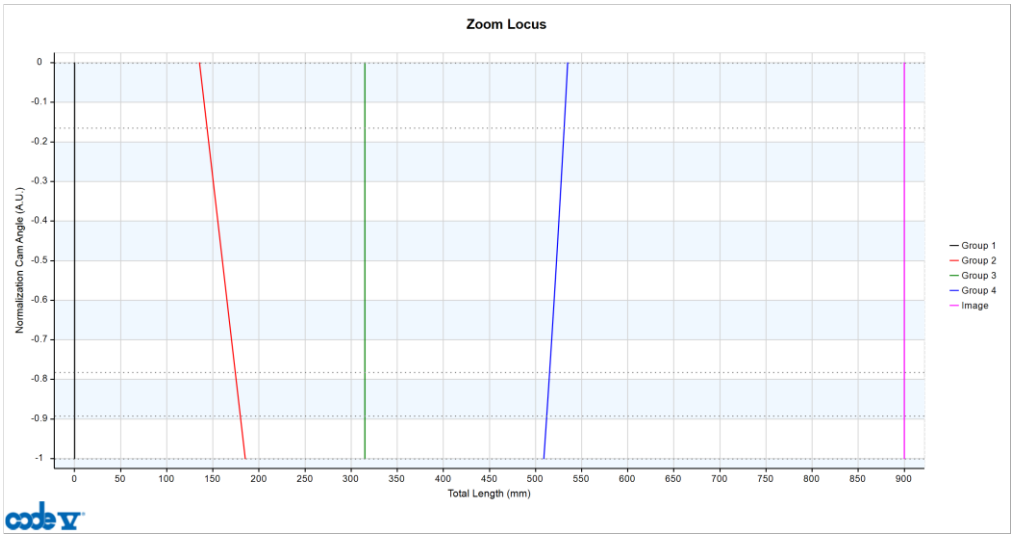

Figure 8. Zoom locus of height-variable zoom lens.

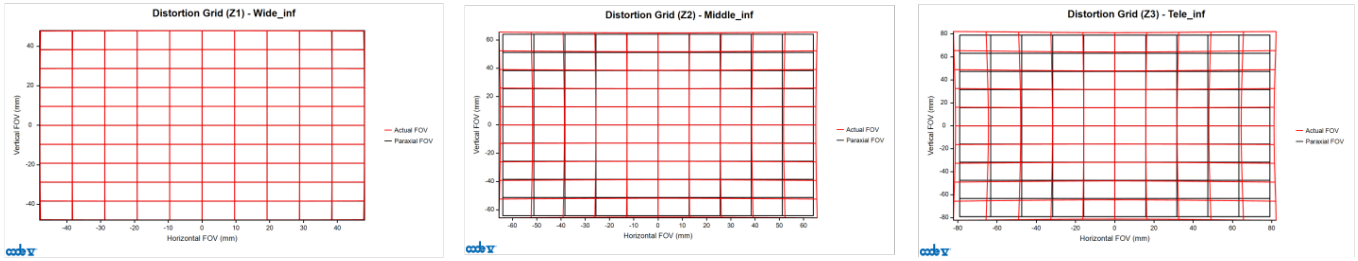

(**a**) (**b**) (**c**)

Figure 9. Distortion grid at object distance infinity at (**a**) wide, (**b**) middle, and (**c**) tele ends.

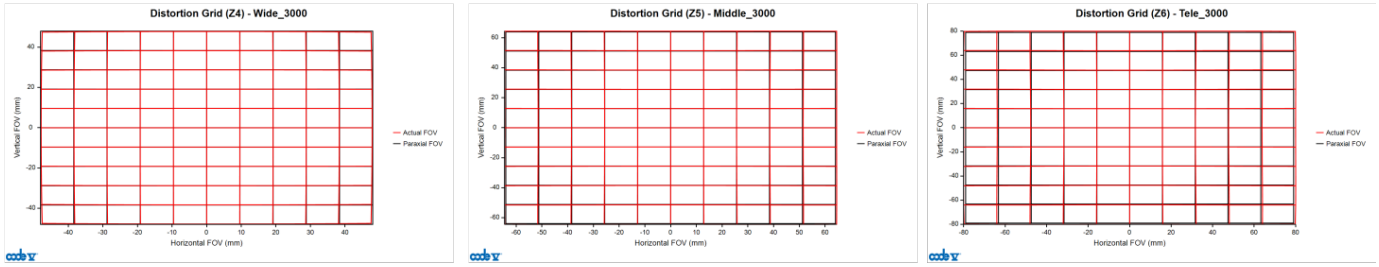

(**a**) (**b**) (**c**)

Figure 10. Distortion grid at an object distance of 3 m at (**a**) wide, (**b**) middle, and (**c**) tele ends.

Figure 9 shows a distortion grid chart for each zoom when the object distance obtained using the CODE V built-in macro is infinite. Figure 9a shows the barrel-type distortion at the wide-angle end. Figure 9b,c show the middle and telephoto ends, respectively, which exhibit a pincushion-type distortion. Figure 9c shows that the distortion was the largest. As the distortion was 4% at the maximum image height, the value was confirmed within 5%, which was the target performance.

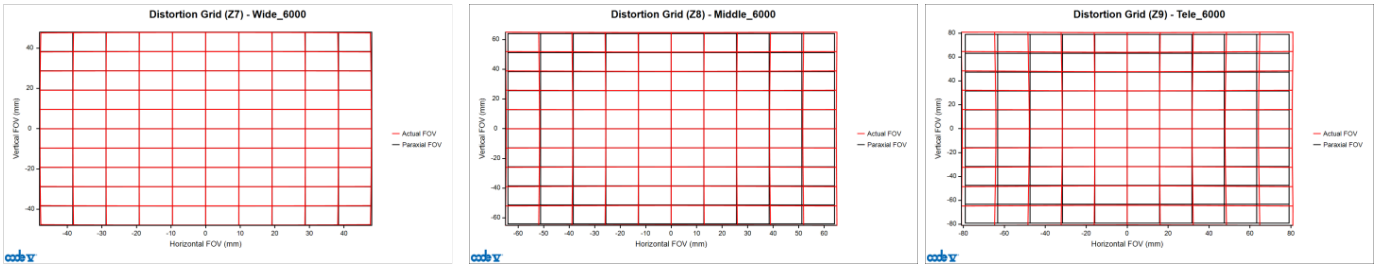

(**a**) (**b**) (**c**)

Figure 11. Distortion grid at an object distance of 6 m at (**a**) wide, (**b**) middle, and (**c**) tele ends.

Even in Figure 10, where the object distance was 3 m, a barrel-type distortion was observed at the wide-angle end (Figure 10a), and the mid-end and telephoto end (Figure 10b,c) had a pincushion-type distortion. Figure 10 shows that the overall distortion was small. Even at the largest wide-angle end (Figure 10a), the distortion was within 1%.

In Figure 11, the wide-angle end picture (Figure 11a) exhibited a barrel-type distortion, whereas the mid-end and telephoto end (Figure 11b,c) had a pincushion-type distortion. The distortion was observed to be the largest at the telephoto end (Figure 11c). Further, the distortion was 2.3%, which was less than the target distortion value.

After checking the distortion in all zooms, the distortion at the telephoto end had the largest value of 4% at the infinite object point in Figure 9. However, the target performance was satisfied because it was within the target distortion of 5%. Because the pixel size of the imaging device was greater than 1 mm, optical aberrations were corrected at the millimeter level through an optimization process.

The resolution was confirmed using a spot diagram. Spot diagrams are a geometric optical jump–spread function. The higher the density, the better is the imaging performance. Because the pixel size of the imaging device in the THz range was 1 mm or more, the device was designed and checked whether the focus was within a boundary of 1 mm $\times$ 1 mm. Parts a, b, and c in Figures 12–14 show the spot diagrams for the wide-angle, middle, and telephoto ends, respectively. The x-axis (the defocus range) was confirmed to be within the range of $\pm$0.05 mm, whereas the y-axis represents the fields of 0, 0.3, 0.5, 0.8, and 1 when the height was standardized to 1. The diffraction MTF (modulation transfer function) was also checked. The x- and y-axes represent spatial frequency (cycles/mm), and the MTF is normalized to one. The block dotted line in F1 represents the diffraction limit.

Figure 12 shows a spot diagram for each zoom at an infinite object point. The minimum value of the wide-angle end (Table 2a) based on defocusing 0 was 0.055 mm in 1 field, and the maximum value was 0.201 mm in 0.8 field. The minimum value of the middle stage (Table 2b) was 0.081 mm in 1 field, and the maximum value was 0.2 mm in 1 field. The minimum value of the telephoto end (Table 2c) was 0.096 mm for 0.5 fields, and the maximum value was 0.297 mm for 1 field. For an infinite object point, the maximum value of the spot was 0.297 mm at the telephoto end, which was smaller than the sensor pixel size of 1 mm. Figure 12b,d,f show the diffraction MTF at infinite points. When the pixel size is 1 mm, the Nyquist frequency is 0.5 cycles/mm, which is close to the diffraction limit of 0.45 at that frequency.

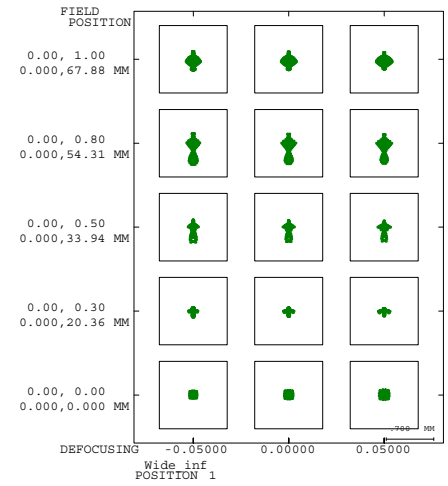

(**a**)

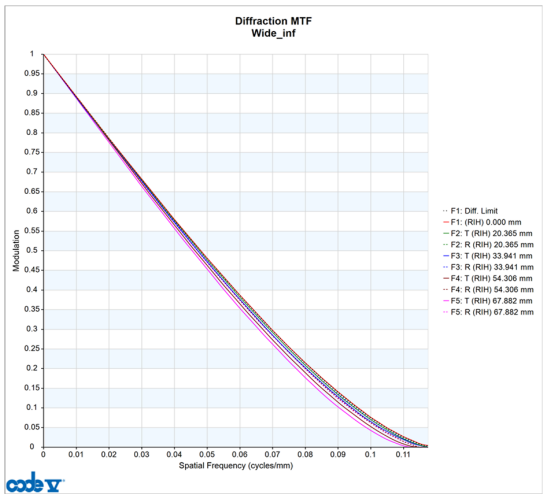

(**b**)

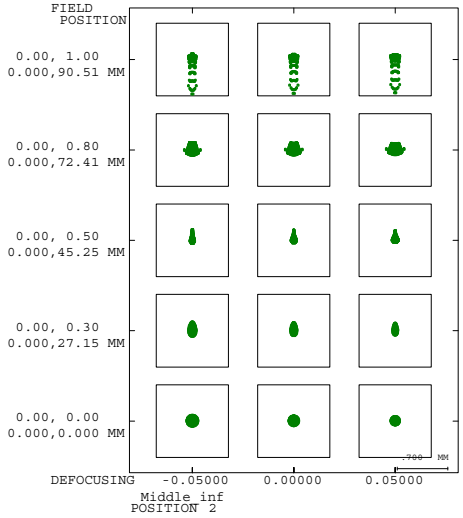

(**c**)

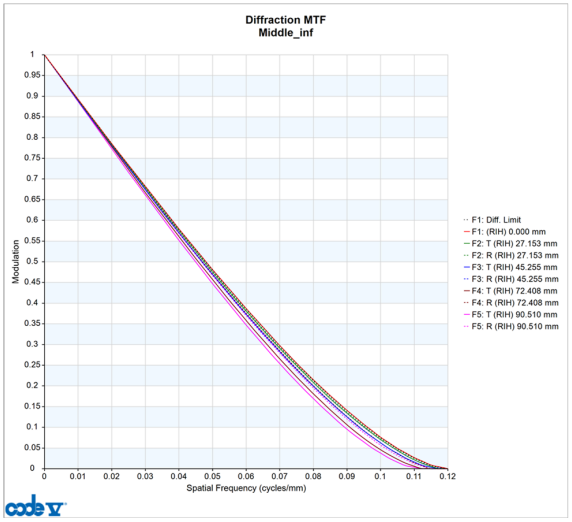

(**d**)

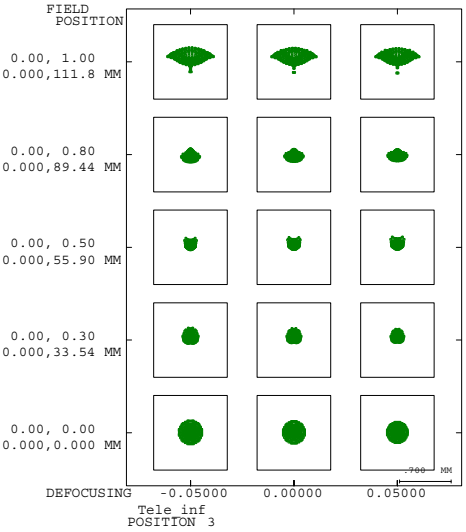

(**e**)

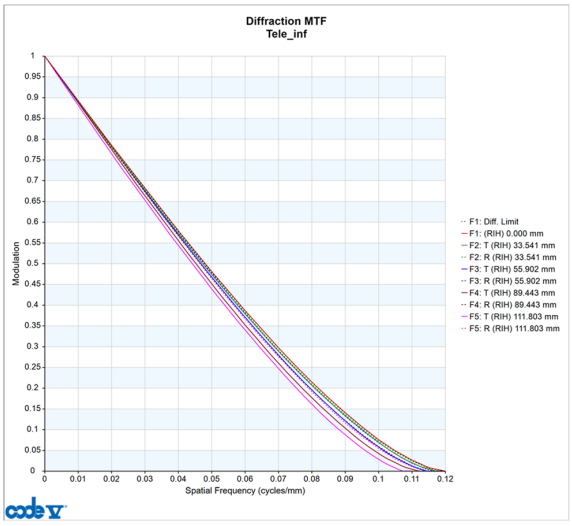

(**f**)

Figure 12. (**a**) Spot diagrams and (**b**) diffraction MTF at infinite object distance for the wide end, (**c**) spot diagrams and (**d**) diffraction MTF at infinite object distance for the middle end, and (**e**) spot diagrams and (**f**) diffraction MTF at infinite object distance for the telephoto end.

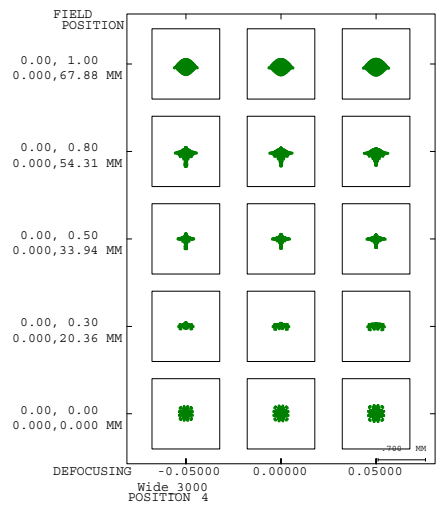

(**a**)

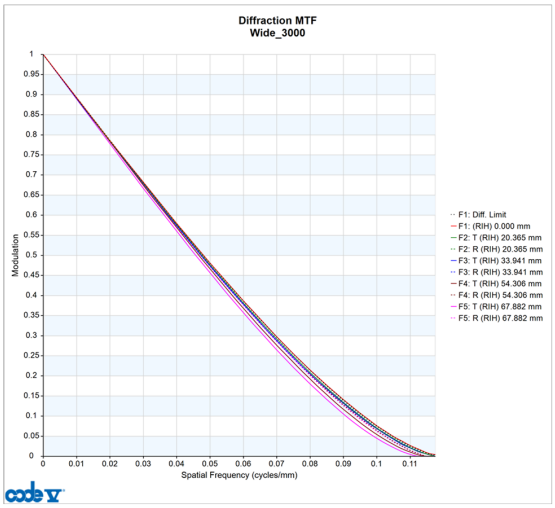

(**b**)

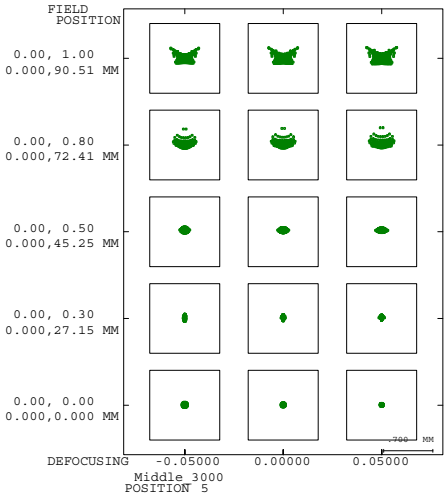

(**c**)

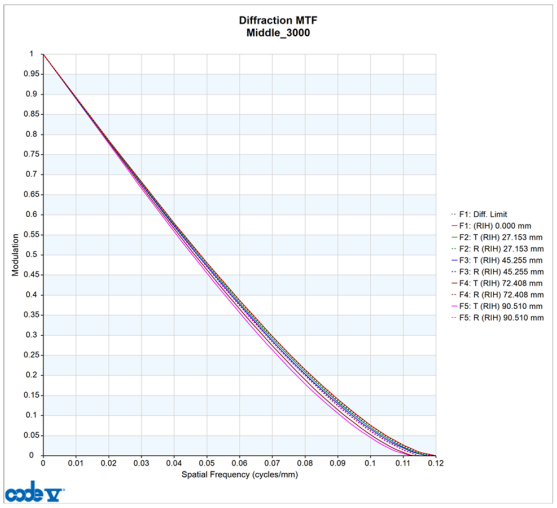

(**d**)

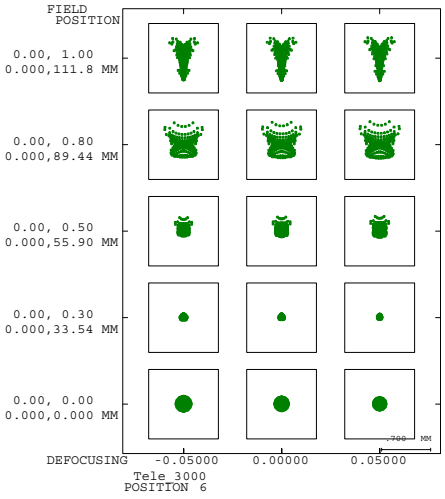

(**e**)

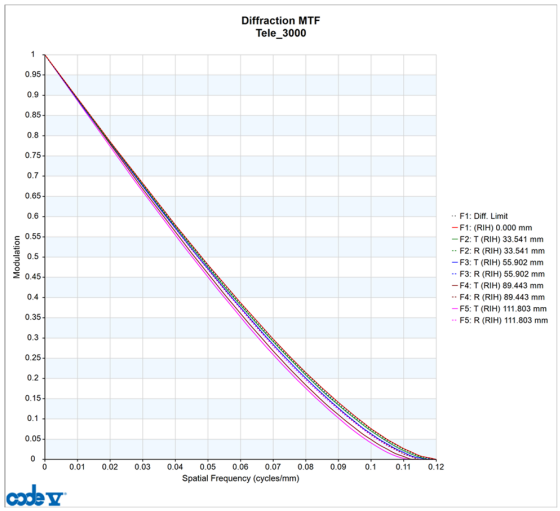

(**f**)

Figure 13. (**a**) Spot diagrams and (**b**) diffraction MTF at an object distance of 3 m for the wide end, (**c**) spot diagrams and (**d**) diffraction MTF at an object distance of 3 m for the middle end, and (**e**) spot diagrams and (**f**) diffraction MTF at an object distance of 3 m for the telephoto end.

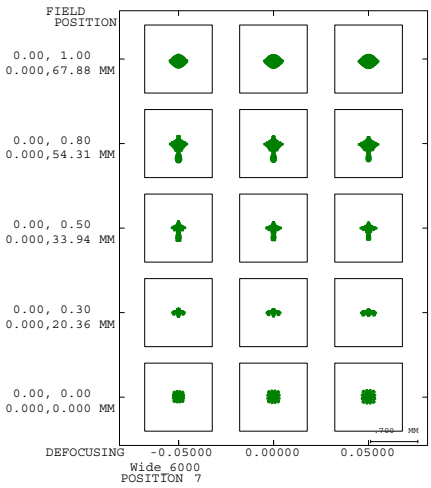

(**a**)

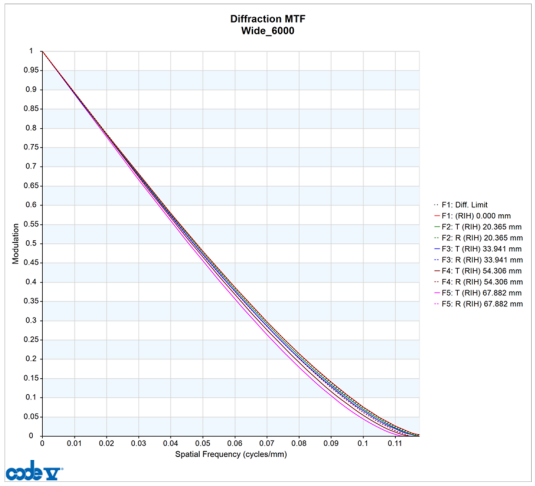

(**b**)

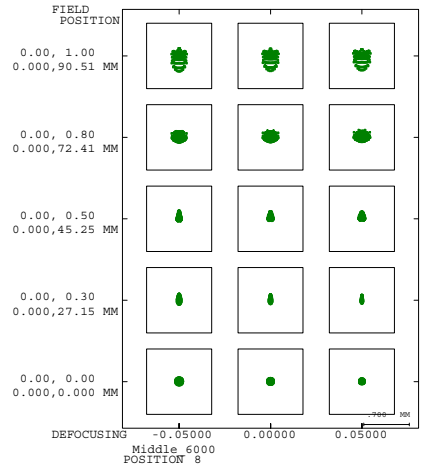

(**c**)

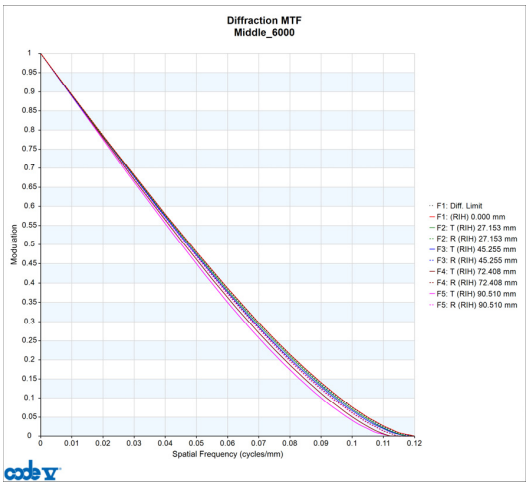

(**d**)

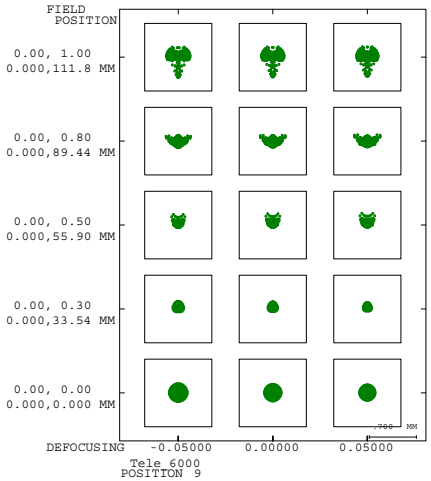

(**e**)

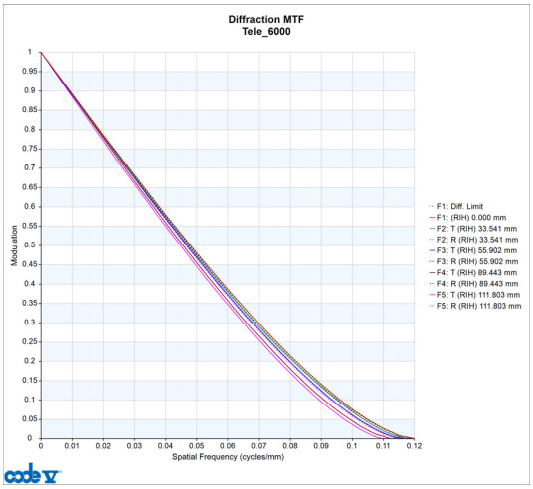

(**f**)

Figure 14. (**a**) Spot diagrams and (**b**) diffraction MTF at an object distance of 6 m for the wide end, (**c**) spot diagrams and (**d**) diffraction MTF at an object distance of 6 m for the middle end, and (**e**) spot diagrams and (**f**) diffraction MTF at an object distance of 6 m for the telephoto end.

Table 2. Image root mean square (RMS) data at object distance infinity.

Field Position	(a) RMS (mm)	(b) RMS (mm)	(c) RMS (mm)
1	0.1542	0.1996	0.2973
0.8	0.2011	0.1453	0.1261
0.5	0.1340	0.0923	0.0955
0.3	0.0610	0.0841	0.1002
0	0.0554	0.0814	0.1575

Figure 13 shows the spot diagrams for each zoom at an object distance of 3 m. The minimum value of the wide-angle end (Table 3a) based on a defocusing of 0 was 0.063 mm at 0.3 field, and the maximum value was 1.90 mm in 1 field. The minimum value for the middle stage (Table 3b) was 0.041 mm in 1 field, and the maximum value was 0.197 mm in 1 field. Further, the minimum value of the telephoto end (Table 3c) was 0.051 mm in 0.3 fields, and the maximum value was 0.326 mm in 1 field. For an object distance of 3 m, the maximum value of the spot was 0.326 mm at the telephoto end, which was smaller than the sensor pixel size of 1 mm. Figure 13b,d,f show the diffraction MTF at 3 m. The performance is close to the diffraction limit of 0.45 at 0.5 cycles/mm.

Table 3. Image RMS data at an object distance of 3 m.

Field Position	(a) RMS (mm)	(b) RMS (mm)	(c) RMS (mm)
1	0.1899	0.1967	0.3259
0.8	0.1556	0.1756	0.2734
0.5	0.1004	0.0788	0.1409
0.3	0.0633	0.0487	0.0509
0	0.0847	0.0409	0.1103

Figure 14 shows a spot diagram for each zoom at an object distance of 6 m. Based on a defocusing of 0, the minimum value of the wide-angle end (Table 4a) was 0.058 mm in 0.3 field, and the maximum value was 0.175 mm in 0.8 field. The minimum value of the middle stage (Table 4b) was 0.06 mm in 1 field, and the maximum value was 0.14 mm in 1 field. The minimum value of the telephoto end (Table 4c) was 0.082 mm in 0.3 field, and the maximum value was 0.216 mm in 1 field. For an object distance of 6 m, the maximum value of the spot was 0.216 mm at the telephoto end, which was smaller than the sensor pixel size of 1 mm. Figure 14b,d,f show the diffraction MTF at 6 m. The performance is close to the diffraction limit of 0.45 at 0.5 cycles/mm.

Table 4. Image RMS data at an object distance of 6 m.

Field Position	(a) RMS (mm)	(b) RMS (mm)	(c) RMS (mm)
1	0.1546	0.1401	0.2161
0.8	0.1746	0.1529	0.1586
0.5	0.1147	0.0870	0.1038
0.3	0.0576	0.0679	0.0818
0	0.0693	0.0604	0.1352

By checking the spot diagrams in Figures 12–14, the spot root mean square (RMS) size was found to be smaller than the pixel size in all zooms, thereby satisfying the target performance. The aberration of the optical system was confirmed at the millimeter level using a spot diagram, and the performance was confirmed using light tools and optical

software (Synopsys Inc.). The designed optical system can show that the diffraction MTF performance values are close to the diffraction limit at all zooms.

An analysis was conducted for object distances of 6 and 3 m. Six zooms were confirmed for the wide-angle, middle, and telephoto ends. The illuminated area resulting from the light-source arrangement was determined according to the magnification of the optical system. The equation for the optical system magnification is derived from the paraxial Snell's law in Equation (8).

$$ni = n'i' \tag{8}$$

Snell's law is referred to as the invariant of refraction because the product of the refractive index and angle of incidence before and after refraction is the same. This can be expressed as Equation (9).

$$ni = n'i' \rightarrow n\frac{y}{l} = n'\frac{y'}{l} \rightarrow n\frac{yh}{l} = n'\frac{y'h}{l} \tag{9}$$

where y is the image height of the chief ray, h is the paraxial image height of the peripheral ray in the thin lens, l is the object distance, and the superscript prime symbol represents the physical quantity after refraction.

$$nuy = n'u'y' \tag{10}$$

The paraxial angle u can be expressed as h/l. Accordingly, Equation (9) can be expressed as Equation (10). In addition, Equation (10) is an invariant whose value does not change before and after refraction and is referred to as a Lagrangian invariant. The equation for the transverse magnification can be derived by modifying the Lagrangian invariant equation.

$$M_T = \frac{y'}{y} = \frac{nu}{n'u'} = -\frac{l'}{l} \tag{11}$$

The magnification of the optical system (M_T) indicates the ratio of the image height y' to the object height y. By organizing Equation (9), the relationship between the refractive index n, paraxial angle u, and the ratio of the object distance and the image distance was expressed, as shown in Equation (11). The entire illumination area was calculated based on the optical system magnification obtained using Equation (11). The sizes of the overall, center, and peripheral receivers were set and placed according to the area. The conduction of lighting analysis using a light source array that matches the number of pixels in the sensor requires a considerable amount of time. All areas need not be checked; it is sufficient to check the performance by checking only the central and peripheral areas. Therefore, a light source array approximately 1/10 times the size of the sensor presented was created in Table 1 and conducted a lighting analysis by placing the light source array in the center and around the actual sensor size (Table 5).

Table 5. Array of light sources used in illuminance analysis.

Detector	Light Source Array	Pixel Size (mm)
Wide	6 × 6	1.5
Middle	10 × 10	1
Tele	20 × 10	1

Figure 15 shows the overall structure of the light sources, receivers, and optical systems for lighting analysis using light tools. The light source array in Figure 14 is a light source array, as presented in Table 5, at the focal position of the optical system, located at the center and periphery of the overall sensor size (Table 1). The optical system was an image-variable system. It is a zoom optical system wherein certain groups moved according to the width, middle, and tele ends. The receiver was installed for the entire lighting area to have a size appropriate for magnification (Table 1) at object distances of 3 and 6 m. To check that the

center and periphery could be enlarged, the center and peripheral receivers were installed in an area enlarged by the magnification of the light source array (Table 5).

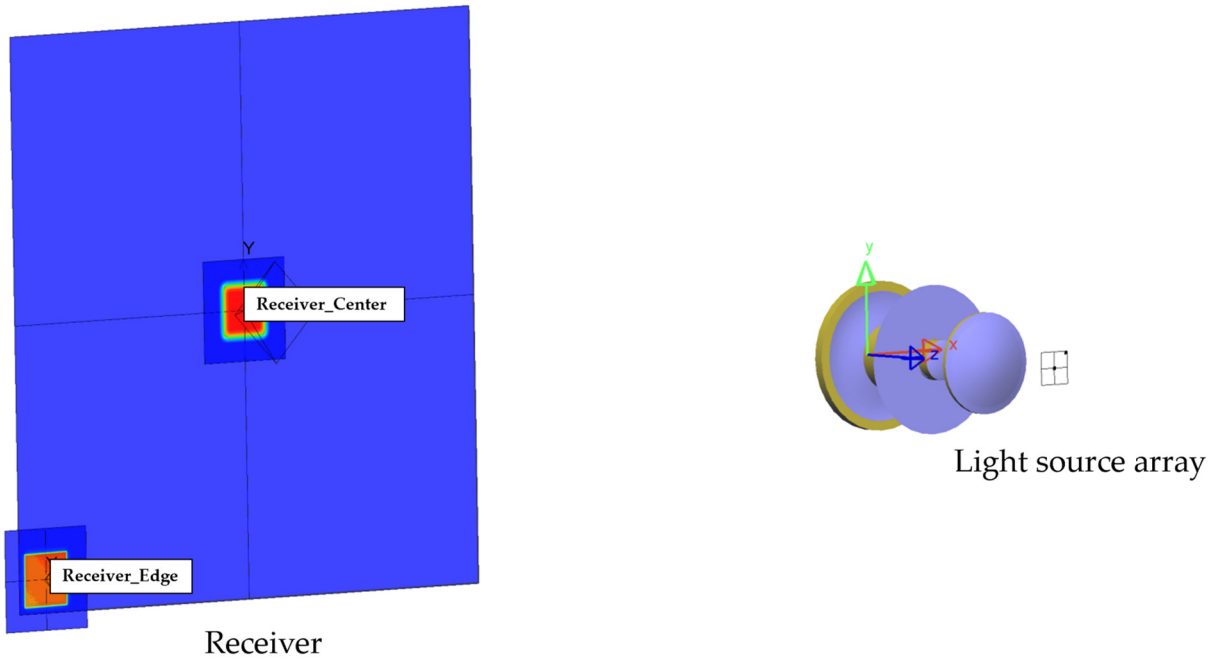

Figure 15. Illuminance analysis system of height-variable zoom lens.

Figures 16 and 17 show the results of the lighting analysis after turning off only certain lights in the diagonal direction to check for the contrast ratio. Figure 16 shows the lighting analysis results at an object distance of 3 m. Figure 16a,b show the results of enlarging the central and peripheral receivers at the wide-angle end. Figure 16c,d show the results of enlarging the receiver in the central and peripheral parts of the middle stages, respectively. Figure 16e,f show the results of enlarging the receiver at the center of the telephoto end and the area around the telephoto end, respectively.

Figure 17 shows the results of the contrast ratio analysis at an object distance of 6 m. Figure 17a,b illustrate the results of enlarging the central and peripheral receivers of the wide-angle end, respectively. Figure 17c,d show the results of enlarging the receiver in the central and peripheral parts of the middle stage, respectively. Figure 17e,f show the results of enlarging the receiver at the center of the telephoto end and the area around the telephoto end, respectively.

The turning off of certain lights in Figures 16 and 17 to check the lighting analysis revealed that one pixel was clearly distinguished in all zoom magnifications, and the contrast ratio for the pixel was high; thus, the performance was satisfactory.

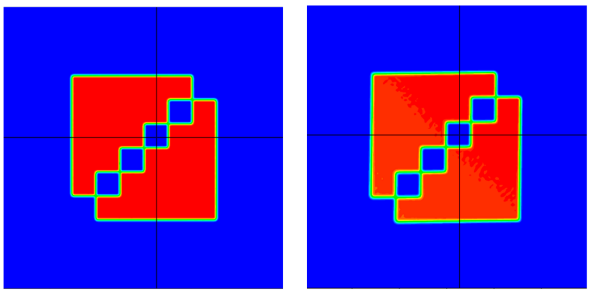

(**a**) (**b**)

Figure 16. *Cont*.

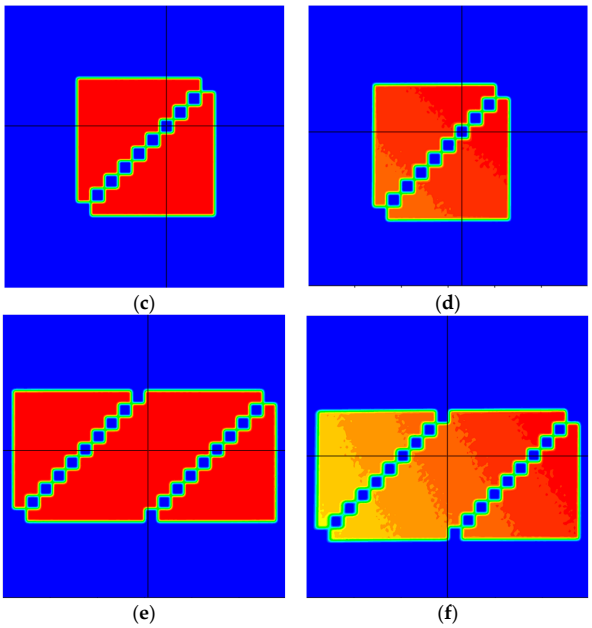

Figure 16. Illuminance analysis results of receiver enlarged in the (**a**) center of the wide angle, (**b**) around the wide angle, (**c**) center of the middle end, (**d**) around the middle end, (**e**) center of the telescope, and (**f**) around the telescope when the object distance is 3 m.

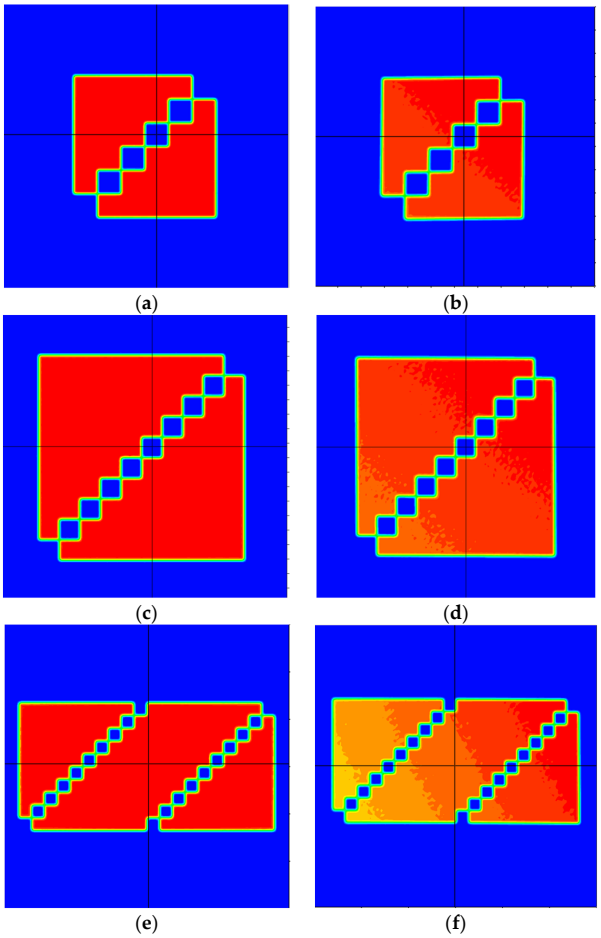

Figure 17. Illuminance analysis results of the receiver enlarged in the (**a**) center of the wide angle, (**b**) around the wide angle, (**c**) center of the middle end, (**d**) around the middle end, (**e**) center of the telescope, and (**f**) around the telescope when the object distance is 6 m.

4. Conclusions

This study designed a novel optical zoom system with a fixed angle of view to support various imaging device sizes for THz applications. To accommodate imaging devices of various sizes, a zoom optical system was constructed wherein the image height was variable, the angle of view was fixed, and the focal length was changed. Based on the optimized design, the lens shape was improved, and aberrations were corrected. The focal length was varied using an internal focus movement method in which the overall length was fixed, and the internal lens group was moved to reduce problems such as driving weight or noise. Because the position of the sensor must be fixed, the focus is adjusted by calculating the amount of movement of the lens group using the zoom equation. Because of the nature of THz waves, their transmittance is very high; therefore, there is a strong possibility that sensor pixels will develop to be larger than 1 mm. Thus, the performance of the optical system was confirmed using a spot diagram. Infinite object points at both 3 and 6 m were confirmed according to the object distance in the spot diagram.

1. The size of the focus was confirmed to be within 1 mm for all zooms at the wide-angle, middle, and telephoto ends. The largest focus was 0.329 mm at the telephoto end when the object distance was 3 m, demonstrating that sufficient results were obtained within 1 mm. The performance was confirmed up to the diffraction limit even when diffraction is considered within the diffraction MTF.

2. Distortion was also checked at infinite object points of 3 and 6 m, depending on the object's distance. The distortion value and grid chart were checked for all zooms at the wide angle, middle, and telephoto ends. For an infinite object point, there was 4% distortion at the telephoto end. When the object distance was 3 m, the maximum distortion was approximately 1% at the wide-angle end. When the object distance was 6 m, the maximum distortion was 2.3% at the telephoto end. The maximum value of the total distortion was 4% for an infinite number of object points, satisfying the target performance within 5%. Because aberrations can be confirmed at the millimeter level, the performance was analyzed using light tools and a lighting optical system software package. The receivers were installed at object distances of 3 and 6 m, and lighting analysis was performed with a light source array at the sensor location. Because the size of the sensor was very large, a light source array of approximately 1/10 the size of the sensor was placed in the center and peripheral portions of the entire sensor size, and the illumination was checked at the central and peripheral receivers.

3. The target lighting area enlarged by the magnification of the sensor was satisfactory for all zooms. The lighting analysis conducted after turning off certain lights indicated that the size of each pixel was clearly distinguished, and the contrast ratio was high in all zooms. Thus, the performance of the inspection optical system was satisfactory. The new optical system proposed in this study can be used regardless of the sensor size, thereby broadening the inspection range.

Author Contributions: Conceptualization, J.P., J.R. and H.C.; methodology, J.P. and J.R.; writing—original draft preparation, J.P., J.R. and H.C. All authors have read and agreed to the published version of the manuscript.

Funding: This work was supported by the Gachon University research fund of 2024 (GCU-202404100001). This work was supported by the Korea Industrial Complex Corporation (KICOX) grant funded by the Korea government (PKB22002).

Institutional Review Board Statement: Not applicable for studies not involving humans or animals.

Informed Consent Statement: Not applicable.

Data Availability Statement: The data presented in this study are included in the article.

Conflicts of Interest: The authors declare no conflicts of interest. The funders had no role in the study design; collection, analyses, or interpretation of data; writing of the manuscript; or decision to publish the results.

Abbreviations

QVGA	Quarter video graphics array
HOF	Half field of view
EFL	Effective focal length
FOV	Field of view
THz	Terahertz
RMS	Root mean square

References

1. Woolard, D.L.; Loerop, W.R.; Shur, M. *Terahertz Sensing Technology: Electronic Devices and Advanced Systems Technology*; World Scientific: London, UK, 2003; Volume 1.
2. Zhang, X.-C.; Xu, J. *Introduction to THz Wave Photonics*; Springer: Berlin, Germany, 2010.
3. Lee, Y.-S. *Principles of Terahertz Science and Technology*; Springer Science & Business Media: Berlin, Germany, 2009.
4. Saeedkia, D. *Handbook of Terahertz Technology for Imaging, Sensing and Communications*; Elsevier: Amsterdam, The Netherlands, 2013.
5. Lewis, R.A. *Terahertz Physics*; Cambridge University Press: Cambridge, UK, 2012.
6. Song, H.-J.; Nagatsuma, T. *Handbook of Terahertz Technologies: Devices and Applications*; CRC Press: Boca Raton, FL, USA, 2015.
7. Dexheimer, S.L. *Terahertz Spectroscopy: Principles and Applications*; CRC Press: Boca Raton, FL, USA, 2017.
8. Das, S.; Nella, A.; Patel, S.K. *Terahertz Devices, Circuits and Systems: Materials, Methods and Applications*; Springer: Berlin, Germany, 2022.
9. Acharyya, A.; Das, P. *Advanced Materials for Future Terahertz Devices, Circuits and Systems*; Springer: Berlin, Germany, 2021.
10. Rieh, J.-S. *Introduction to Terahertz Electronics*; Springer Nature: Berlin, Germany, 2020.
11. Coutaz, J.-L.; Garet, F.; Wallace, V. *Principles of Terahertz Time-Domain Spectroscopy*; CRC Press: Boca Raton, FL, USA, 2018.
12. Ganichev, S.; Prettl, W. *Intense Terahertz Excitation of Semiconductors*; Oxford University Press: New York, NJ, USA, 2005.
13. Rogalski, A. *Infrared and Terahertz Detectors*; CRC Press: Boca Raton, FL, USA, 2019.
14. Kingslake, R.; Johnson, R.B. *Lens Design Fundamentals*; Academic Press: Cambridge, MA, USA, 2009.
15. Pedrotti, F.L.; Pedrotti, L.M.; Pedrotti, L.S. *Introduction to Optics*; Cambridge University Press: Cambridge, UK, 2017.
16. Kim, K.M.; Choe, S.-H.; Ryu, J.-M.; Choi, H. Computation of Analytical Zoom Locus Using Padé Approximation. *Mathematics* **2020**, *8*, 581. [CrossRef]
17. Smith, G.H. *Practical Computer-Aided Lens Design*; Willmann-Bell, Incorporated: Richmond, VA, USA, 1998.
18. Laikin, M. *Lens Design*; CRC Press: Boca Raton, FL, USA, 2006.
19. Lo, Y.H.; Leonhardt, R. Aspheric lenses for terahertz imaging. *Opt. Express* **2008**, *16*, 15991–15998. [CrossRef] [PubMed]
20. Jiang, X.-Y.; Ye, J.-S.; He, J.-W.; Wang, X.-K.; Hu, D.; Feng, S.-F.; Kan, Q.; Zhang, Y. An ultrathin terahertz lens with axial long focal depth based on metasurfaces. *Opt. Express* **2013**, *21*, 30030–30038. [CrossRef] [PubMed]
21. He, J.; Ye, J.; Wang, X.; Kan, Q.; Zhang, Y. A broadband terahertz ultrathin multi-focus lens. *Sci. Rep.* **2016**, *6*, 28800. [CrossRef] [PubMed]
22. Zhang, Z.; Zhang, H.; Wang, K. Diffraction-free THz sheet and its application on THz imaging system. *IEEE Trans. Terahertz Sci. Technol.* **2019**, *9*, 471–475. [CrossRef]
23. Harris, Z.B.; Katletz, S.; Khani, M.E.; Virk, A.; Arbab, M.H. Design and characterization of telecentric f-θ scanning lenses for broadband terahertz frequency systems. *AIP Adv.* **2020**, *10*, 125313. [CrossRef] [PubMed]
24. Gao, Y.; Gu, J.; Jia, R.; Tian, Z.; Ouyang, C.; Han, J.; Zhang, W. Polarization independent achromatic meta-lens designed for the terahertz domain. *Front. Phys.* **2020**, *8*, 606693. [CrossRef]
25. Shamuilov, G.; Domina, K.; Khardikov, V.; Nikitin, A.Y.; Goryashko, V. Optical magnetic lens: Towards actively tunable terahertz optics. *Nanoscale* **2021**, *13*, 108–116. [CrossRef]
26. Jia, W.; Lou, M.; Gao, W.; Sensale-Rodriguez, B. Design and fabrication of a terahertz dual-plane hologram and extended-depth-of-focus diffractive lens. *Opt. Contin.* **2022**, *1*, 1722–1729. [CrossRef]
27. Gross, H.; Blechinger, F.; Achtner, B. *Handbook of Optical Systems*; Wily-VCH Verlag GmbH & Co.: Hoboken, NJ, USA, 2005.
28. Fischer, R.; Tadic-Galeb, B.; Yoder, P. *Optical System Design*; McGraw-Hill Education: New York, NJ, USA, 2008.
29. Singer, W.; Totzeck, M.; Gross, H. *Handbook of Optical Systems, Physical Image Formation*; John Wiley & Sons: Hoboken, NJ, USA, 2006.
30. Stotts, L.B. *Free Space Optical Systems Engineering: Design and Analysis*; John Wiley & Sons: Hoboken, NJ, USA, 2017.
31. Jung, U.; Choi, J.H.; Choo, H.T.; Kim, G.U.; Ryu, J.; Choi, H. Fully Customized Photoacoustic System Using Doubly Q-Switched Nd: YAG Laser and Multiple Axes Stages for Laboratory Applications. *Sensors* **2022**, *22*, 2621. [CrossRef] [PubMed]
32. Osten, W. *Optical Inspection of Microsystems*; CRC Press: Boca Raton, FL, USA, 2019.
33. Choi, H.; Ju, Y.J.; Jo, J.H.; Ryu, J.-M. Chromatic aberration free reflective mirror-based optical system design for multispectral photoacoustic instruments. *Technol. Health Care* **2019**, *27*, 397–406. [CrossRef] [PubMed]
34. Choi, H.; Ryu, J.-M.; Choe, S.-W. A novel therapeutic instrument using an ultrasound-light-emitting diode with an adjustable telephoto lens for suppression of tumor cell proliferation. *Measurement* **2019**, *147*, 106865. [CrossRef]
35. Seo, S.H.; Ryu, J.M.; Choi, H. Focus-Adjustable Head Mounted Display with Off-Axis System. *Appl. Sci.* **2020**, *10*, 7931. [CrossRef]

36. Welford, W.T. *Aberrations of Optical Systems*; CRC Press: Boca Ration, FL, USA, 1986.
37. Smith, W.J. *Modern Lens Design*; McGraw-Hill: New York, NJ, USA, 2005.
38. Twyman, F. *Prism and Lens Making: A Textbook for Optical Glassworkers*; Routledge: Abingdon-on-Thames, UK, 2017.